Using machine-learning to construct TOMCAT model and occultation measurement-based stratospheric methane (TCOM-CH4) and nitrous oxide (TCOM-N2O) profile data sets

Sandip S. Dhomse[1,2] and Martyn P. Chipperfield[1,2]

[1]School of Earth and Environment, University of Leeds, Leeds, UK
[2]National Centre for Earth Observation, University of Leeds, Leeds, UK

Correspondence: Sandip Dhomse (s.s.dhomse@leeds.ac.uk)

Abstract. Monitoring the atmospheric concentrations of greenhouse gases (GHGs) is crucial ~~in order~~ to improve our understanding of their climate impact. However, there are no long-term profile data sets of important GHGs that can be used to gain a better insight into the processes controlling their variations in the atmosphere. ~~Here, we merge~~ In this study, we apply corrections to the chemical transport model (CTM) output ~~and~~ based on the profile measurements from two solar occultation instruments~~,~~: the HALogen Occultation Experiment (HALOE) and the Atmospheric Chemistry Experiment - Fourier Transform Spectrometer (ACE-FTS)~~,~~. The goal is to construct long-term (1991-2021), gap-free stratospheric profile data sets~~(hereafter, TCOM)~~ , hereafter referred to as TCOM, for two important GHGs. ~~The Extreme Gradient Boosting (XGBoost) regression model is used to~~

To estimate the corrections needed to apply to the CTM profiles, we use the Extreme Gradient Boosting (XGBoost) regression model. For methane (TCOM-CH4), we ~~use~~ utilize both HALOE and ACE satellite profile measurements ~~(1992-2018) to~~ from 1992 to 2018 to train the XGBoost model, while profiles from ~~three later years (2019-2021) are used~~ 2019 to 2021 serve as an independent evaluation data set. As there are no nitrous oxide (N_2O) profile measurements for earlier years, we derive XGBoost-derived correction terms to construct TCOM-N2O profiles ~~are derived~~ using only ACE-FTS profiles ~~for~~ from the 2004-2018 time period, with profiles from 2019-2021 ~~again being~~ used for the independent evaluation.

Overall, both TCOM-CH4 and TCOM-N2O profiles ~~show~~ exhibit excellent agreement with the available satellite measurement-based data sets. We find that compared to evaluation profiles, biases in TCOM-CH4 and TCOM-N2O are generally less than 10% and 50%, respectively, throughout the stratosphere. ~~Daily~~ The daily zonal mean profile data sets~~on altitude (15–60 km~~, covering altitude (15–60km) and pressure (300–0.1 hPa) levels, are publicly available via the following links: https://doi.org/10.5281/zenodo.7293740 for TCOM-CH4 (Dhomse, 2022a) and https://doi.org/10.5281/zenodo.7386001 for TCOM-N2O (Dhomse, 2022b).

1 Introduction

After carbon dioxide (CO_2), methane (CH_4) and nitrous oxide (N_2O) are currently the two most important anthropogenically emitted greenhouse gases (GHGs) and their concentrations in the atmosphere are increasing at substantial rates (e.g.

Meinshausen et al., 2020). Primary natural sources of CH_4 are wetlands, decay of organic waste and livestock whereas anthropogenic sources include landfills and production and transport of coal, natural gas and oil (e.g. Saunois et al., 2016; Lan et al., 2021). The primary emission sources for N_2O are agricultural practices, industrial activities, combustion of fossil fuels and treatment of solid/liquid waste (e.g. Tian et al., 2020). Importantly, as measured by the global warming potential (GWP), CH_4 is about 25 times and N_2O is about 300 times more potent as GHGs compared to CO_2.

The lifetime of CH_4 in the troposphere is about 9 years (e.g. Lelieveld et al., 1998), and it is primarily removed through oxidation by OH. However, in the stratosphere CH_4 destruction is much slower, hence its local lifetime increases to about 150 years (Chipperfield et al., 2013). CH_4 oxidation is also an important source of water vapour in the stratosphere which plays a key role in ozone chemistry via HOx cycles, thereby it also influences the radiative balance in the middle stratosphere. The primary atmospheric sink for N_2O is photolysis (producing N_2 + O) in the stratosphere/mesosphere, therefore it is also a long-lived species (lifetime about 120 years (Chipperfield et al., 2013)). A secondary sink for N_2O is reaction with $O(^1D)$ to produce NO that plays a key role in the middle atmosphere O_3 budget via the NOx cycle. An important aspect is that increases in both OH and NO can have also have positive impact on ozone especially in the lower stratosphere, as they help to convert reactive species to long-lived reservoir species. For example, OH + NO_2 (+ M) leads to HNO_3 formation while CH_4 + Cl leads to HCl formation, reducing concentrations of reactive NO_2 and Cl. Additionally, as both CH_4 and N_2O are long-lived in the stratosphere, monitoring their concentrations also help us to understand changes in stratospheric chemistry and dynamics.

However, despite their importance, there are only a few satellite instrument that provide global stratospheric profiles of CH_4 or N_2O. Relatively long-term and high quality data records are available from two solar occultation instruments, the HALogen Occultation Experiment (HALOE) and the Atmospheric Chemistry Experiment-Fourier Transform Spectrometer (ACE-FTS), and limb sounding instruments such as the Michelson Interferometer for Passive Atmospheric Sounding (MIPAS) and the Microwave Limb Sounder (MLS). However, each instrument has different spatial and temporal coverage and they use different measurement techniques and retrieval algorithms. Hence merging these satellite data to construct a single long-term data set for a given species is quite challenging.

Therefore, although stratospheric CH_4 and N_2O profile data sets were released recently by Hegglin et al. (2021), they did not attempt to merge data from different satellite instruments. Briefly, these data sets were released as part of the Stratospheric and Tropospheric Processes And their Role in Climate (SPARC) Data Initiative, and contain monthly mean zonal mean profiles in volume mixing ratio (vmr) units on pressure levels. Data from individual satellite instruments are averaged at 36 latitude bins (2.5° latitudinal resolution) and provided on 26 pressure levels ranging from 300 hPa to 0.1 hPa. SPARC CH_4 profile data is constructed using ACE-FTS (2004–2019), HALOE (1991–2005) and MIPAS (2002–2012) satellite instrument measurements (Hegglin et al., 2020). Note that SPARC data uses earlier (v3.6) version of the ACE-FTS data For N_2O there is no data set for the 1990s but for later periods SPARC N_2O data contains monthly mean values from Aura-MLS (based on v4.2), MIPAS (v224), ~~MIPAS,~~ the Sub-Millimetre Radiometer (SMR, v2.1), and ACE-FTS measurements. Monthly means values are available only if there are more than five valid profiles for a given latitude/altitude range. Monthly mean files are available for individual instruments and there is no merging or adjustment for different data sets.

To our knowledge, until now no attempt has been made to merge satellite data records to construct long-term stratospheric CH_4 and N_2O profile data sets. Here, we do this by constructing correction terms for the stratospheric CH_4 and N_2O profiles from a chemical transport model by analysing the difference between the model and available satellite observations. Then, the correction terms (i.e. difference needed to adjust TOMCAT CH_4/N_2O profiles) are calculated for all the model grid points to construct a long-term, gap-free stratospheric profile data set. Details of the satellite data and model set up used here are described in Sections 2 and 3, respectively. The methodology used to estimate correction terms is described in Section 4. Evaluation of the newly constructed data set for CH_4 and N_2O is presented in Section 5, followed by Summary and Conclusions in Section 6.

2 Satellite data and model setup

Being potent GHGs and primary sources of stratospheric water vapour and NOx, stratospheric CH_4 and N_2O measurements gained scientific attention even before the discovery of the Antarctic ozone hole (Farman et al., 1985). Initial measurements were performed by the Stratospheric and Mesospheric Sounder (SAMS) instruments on Nimbus 7 satellite that was launched in 1978 (Drummond et al. (1980); Jones and Pyle (1984)). Similarly, the Atmospheric Trace Molecule Spectroscopy (ATMOS) instrument (Gunson et al., 1990) provided about 350 profiles during four space shuttle missions (in 1985, 1992, 1993 and 1994). Later, the Improved Stratospheric and Mesospheric Sounder (ISAMS) was able to provide about 2600 profiles/day for about 180 days between 1991-1992, but retrieval was feasible only for the upper stratospheric/mesospheric altitude range (e.g. Remedios et al., 1996).

A step-change in the number of stratospheric CH_4 measurements occurred with the deployment of HALOE on the Upper Atmosphere Research Satellite (UARS) in September 1991, followed by ACE-FTS in August 2003. Both instruments provided about 30 profiles per day (discussed below). Two additional instruments, SCIAMACHY (SCanning Imaging Absorption spectroMeter for Atmospheric CHartographY) and MIPAS on the Envisat satellite platform also provided useful stratospheric CH_4 profiles over the 2003–2012 time period (e.g. Noël et al., 2016, 2018). For N_2O, the Cryogenic Limb Array Etalon Spectrometer (CLAES) on the UARS satellite platform provided about one year of profile measurements (October 1991 to July 1992). Later, the Sub-Millimetre Radiometer (SMR) on Odin, launched in 2001 (e.g. Urban et al., 2005), MIPAS, and the Microwave Limb Sounder (MLS) on the Aura satellite (Waters et al., 2006) also provided very useful N_2O profile measurements. However, to avoid inter-instrument biases likely due to differences in the measurement techniques, we decided here to use only HALOE and ACE-FTS data.

2.1 HALOE

HALOE was launched aboard UARS in September 1991 (Russell III et al., 1993). The spacecraft was in a 57° inclined orbit at an altitude of ∼585 km that allowed for observations from 80°S to 80°N. The HALOE instrument used a combination of broadband radiometry and gas filter correlation techniques to observe several trace gas species in the spectral range of 2.410.4 μm (or 963–4140 cm^{-1}). HALOE provided about 30 measurements (15 sunrise and 15 sunset) per day with near-global

coverage in approximately one month. In general, daily measurements are provided at two nearly fixed latitudes (sunrise and sunset) with near equal longitude spacing. For CH_4 the retrieval algorithm uses a 2855–2915 cm^{-1} spectral window (channel 6) and profiles are retrieved for the 15 km to 90 km range. The algorithm uses an onion-peel scheme with 1.5 km thick tangent layer to calculate the transmission using a forward model thereby achieving about 1.5 km vertical resolution. Here we use HALOE v19 data that is available for October 1991 to November 2005 time period and is obtained via https://acdisc.gesdisc.eosdis.nasa.gov/data//UARS_HALOE_Level2/.

2.2 ACE-FTS

ACE-FTS was launched aboard the SciSat-1 spacecraft in August 2003 (Bernath, 2002). The spacecraft was launched in a drifting orbit at an inclination of 74° which allows for observations from to 85°S to 85°N. The ACE-FTS instrument has very high spectral resolution (0.02 cm^{-1}) and covers the spectral range between 750 and 4400 cm^{-1} (Bernath et al., 2005). Similar to HALOE, ACE-FTS uses the solar occultation technique (30 measurements per day). Global latitude coverage is obtained over a period of 3 months and is almost exactly periodic from year to year. The CH_4 profile retrieval uses about 60 microwindows between 1244–3087 cm^{-1} while the N_2O retrieval uses 69 microwindows between 1120-2600 cm^{-1} (Strong et al., 2008). Retrieval is performed at 1 km resolution from about 5 km to 70 km (Boone et al., 2020). It is important to note that ACE retrieval does not use averaging kernel as it uses so called global analysis type approach where all data are fitted simultaneously using Levenberg-Marquardt least squares methods. It means vmr for all the contributing molecules in a given microwindow set are fitted/retrieved simultaneously, which is different than onion-peeling method adopted for HALOE retrieval. Here we use ACE v4.2 data that is obtained via http://www.ace.uwaterloo.ca/data.php

3 TOMCAT CTM

As both CH_4 and N_2O are long-lived tracers in the stratosphere, their stratospheric distributions are largely determined by transport process. Hence, we decided to use profiles simulated by TOMCAT CTM as it is forced with most up-to-date meteorological reanalysis data set. Briefly, TOMCAT is an off-line three-dimensional CTM that includes a comprehensive stratospheric chemistry scheme but, in the version used here, with a simple tropospheric chemical scheme (Chipperfield, 2006). This means concentrations of long-lived ozone depleting substances (ODSs) and GHGs are prescribed as surface mixing ratio boundary conditions (e.g. WMO, 2018) and are assumed to be well mixed throughout the troposphere. For CH_4 the model uses observed monthly mean global surface concentrations from the National Oceanic and Atmospheric Administration (NOAA) network. The CTM setup is therefore similar to the control simulations used in our recent studies such as Dhomse et al. (2022) and Li et al. (2022). The model simulation is performed at a 2.8° × 2.8° horizontal resolution with 32 hybrid sigma-pressure levels (surface to about 60 km) and is forced with ERA5 (and ERA5.1) reanalysis meteorology (Hersbach et al., 2020). The effects of time-varying solar flux changes and volcanically enhanced stratospheric aerosol are included by using separate time-varying forcing files (e.g. Dhomse et al., 2015, 2016).

4 Methodology

For stratospheric ozone various methodologies have been adopted to merge different types of data to construct homogenised data sets. They include both simple and complex methodologies for adjusting biases for overlapping time periods (e.g. Hassler et al., 2008, 2018; Arosio et al., 2018), use of multivariate linear model (e.g. Randel and Wu, 2007) and data assimilation (Inness et al., 2015). However, we are not aware of any attempt to construct long-term stratospheric CH_4 and N_2O profile data sets using different satellite data sets.

Here, our approach is similar to that of Dhomse et al. (2021) for ozone who used CTM profiles as a transfer function and estimated model-observation biases using machine learning. However, they used observation-based monthly mean zonal mean ozone values from ~~SWOOSH data set~~ Stratospheric Water and OzOne Satellite Homogenized (SWOOSH) data set (Davis et al., 2016) rather than individual satellite data products. As there are a number of satellite instruments that provide ozone profile measurements, monthly mean zonal mean values in merged ozone data sets are considered to be well constrained. However, as noted in Section 2, there are very few satellite instruments that provide CH_4 profile measurements (largely two occultation instruments providing 30 profiles per day), so we decided to use individual data points to train a machine learning algorithm. Similarly, for N_2O (among ~~occulatation~~ occultation instruments) only ACE-FTS provides a long profile data record, but again it has limited spatial coverage hence calculation of monthly mean zonal mean profiles are subject to sampling errors.

Overall, there are 6 steps in our approach. First, TOMCAT output fields are sampled for HALOE and ACE measurement collocations. There are about 95,000 HALOE profiles and over 106,000 ACE profiles in the 1991-2021 time period. Second, as ACE profiles are available at 1 km vertical resolution, HALOE profiles are also binned at 1 km vertical resolution and TOMCAT profiles (surface to 60 km) are interpolated to the same grid.

Third, we calculate observation-TOMCAT profile differences for each 1 km grid and satellite measurements are included only if retrieval errors are less than 100% ~~.~~ and retrieved values are greater than zero. Note that we assume that all the measurements with retrieval errors less that 100% are more or less absolute truth. Hence, no other uncertainties are considered in the further calculations. Out attempt is to construct profile data that would approximate HALOE/ACE data if the instruments had denser measurements without any temporal gaps. As there are distinct dynamical (and chemical) regimes in the stratosphere in terms of processes controlling distribution of these two GHGs, we divide global measurements into five latitude bins: southern hemisphere (SH) polar (SHpol, 50°S-90°S), SH mid-latitude (SHmid, 20°S-70°S), tropical (40°S-40°N), northern hemisphere (NH) mid-latitude (NHmid, 20°N-70°N) and NH polar (NHPol, 50°N-90°N). A 20° (10° from either side) latitudinal overlap between the bins is allowed to include possible extreme variations in the training data set. Estimated differences for overlapping grids are averaged in order to avoid possible sharp edges near the latitude bin boundaries.

Fourth, we train the XGBoost regression model for TOMCAT-observation differences of CH_4 or N_2O for each vertical level. This means there is a separate model for each vertical level (46 for 15-60 km) for each of the 5 latitudinal bins. Briefly, XGBoost is a supervised machine learning algorithm that uses an ensemble of decision trees (e.g. Chen and Guestrin, 2016). XGBoost applies the principle of boosting weak learners using the gradient descent architecture (Gradient Boosting) with some additional components such as L1 and L2 (Lasso and Ridge) regularization that helps to prevent over-fitting. There

are 13 explanatory variables (or features) in our XGBoost regression model taken from TOMCAT output fields or the ERA5 reanalyses used to force the model. For example, the XGBoost regression model for CH_4 can be represented as:

$$dCH_4 = \beta_1 CH_4 + \beta_2 O_3 + \beta_3 N_2O + \beta_4 HNO_3 + \beta_5 HCl + \beta_6 H_2O + \beta_7 HF + \beta_8 NO_2 + \beta_9 ClONO_2 + \beta_{10} temperature T + \beta_{11} PV + \beta_{12} latitude \Theta + \beta_{13} time t + errors \epsilon \quad (1)$$

where ~~potential vorticity (PV) and temperature are~~ T and PV are temperature and potential vorticity from ERA5 at co-located TOMCAT grid points. ~~Latitude and time~~ Measurement latitude (Θ) and date (t) variables are included to represent temporal/spatial variations in the measurements, whereas ϵ denotes unexplained errors. Variables β_1 to β_{13} can be considered as the contribution coefficient for a given explanatory variable. For CH_4, we include an additional (14^{th}) step-function-like term in the XGBoost model that is set to 0 for the HALOE time period and 1 for the ACE-FTS time period. Our approach here is to assume that nearly all differences in the TOMCAT CH_4 or N_2O profiles with respect to HALOE and ACE data arise from the incorrect representation of the chemical and dynamical processes in the CTM (including inhomogeneities in ERA5 data that are used to drive TOMCAT transport). Our aim is to find correction terms for the TOMCAT CH_4 or N_2O profiles so that they match observational profiles for a particular distribution of model tracers and dynamical set up. Hence, we include nine tracers of varied lifetimes (i.e. CH_4, O_3, N_2O, HNO_3, HCl, H_2O, HF, N_2O, $ClONO_2$) from TOMCAT. We are aware that some tracers are correlated as all the variables are from a TOMCAT simulation (or forcing meteorology), hence we use Lasso (L1) regularisation option to remove less important variables in case one or some of them are highly correlated at a particular level. We use Python package XGBoost (https://xgboost.readthedocs.io/en/stable/python/python_intro.html) for the analysis with following options: n_estimators=1000, max_depth=4, alpha=0.3, learning_rate=0.1, min_child_weight=6. As mentioned earlier, profiles prior to 2018 are used for training (70%) and testing (30%) XGBoost for individual vertical levels. As an additional check, we use the last three years (2019–2021) of data points for the evaluation.

Fifth, we sample daily TOMCAT output at 1.30~~am and 1.30 pm~~ and 13.30 UTC equatorial crossing times (day and night time sampling). TOMCAT 3D fields are then re-gridded at 1 km vertical resolution before dividing them into five latitude bins (see above). Trained XGBoost regression models are then used to calculate correction terms for all twice-daily 3D output profiles.

Sixth, correction terms for individual model grid points are merged to construct twice daily (~~day~~1.30 and 13.30 UTC) 3D (longitude/~~night time~~latitude/height) correction terms. As mentioned above, we use use simple averaging for the overlapping grid points to avoid sharp boundaries, followed by simple 2-dimensional (latitude-longitude) smoothing using 3-point boxcar smoothing. These twice daily correction terms are then added to the original TOMCAT CH_4 and N_2O profiles~~to produce~~. Daily mean 3D (longitude/latitude/height) correction terms are calculated by averaging 1.30 and 13.30 UTC fields, followed by zonal means (latitude/height) to produce daily mean zonal mean TCOM-CH4 and TCOM-N2O profiles.

5 Results

As noted in the Introduction, CH_4 and N_2O concentrations in the lower stratosphere are largely controlled by dynamical processes. The reanalysis data sets used to drive transport in the CTM can be considered as our best knowledge of the past atmosphere as they attempt to incorporate most of the available high quality meteorological observations using data assimilation. However, they are prone to issues related to changes in the number and type of observations assimilated in the reanalysis system, which might introduce ~~homogeneities~~ inhomogeneities in the data sets produced. On the other hand, although chemical models are ideal tools for simulating and understanding past changes in these two greenhouse gases using consistent chemical schemes, they are also prone to deficiencies. For example, some computationally expensive processes (e.g. vertical mixing in the troposphere) are represented by somewhat simplified parameterisations. Additionally, most of the chemical reaction rates (loss rates) calculated in the model scheme can also have large uncertainties. Hence, chemical-transport-model-simulated profiles often show some kind of bias with respect to observational data sets. Similarly, although occultation-technique-based instruments measure atmospheric spectra at relatively high resolution, they also include simplified parameterisations for complex radiative processes (e.g. scattering, contribution from interfering gases) and so retrieval errors are also sensitive to changes in stratospheric conditions. Hence, here we assume that some of the differences between TOMCAT and observations could be attributed to the distribution of other TOMCAT tracers. We use XGBoost to identify possible interconnection patterns between TOMCAT CH_4 or N_2O differences and other tracers using available data points so that corrections can be estimated for all model grid points.

Figure 1 shows vertical profiles of estimated variance (R^2) and feature (explanatory variable) importances for the SHpol (50°S-90°S) latitude bin for the XGBoost regression model. Feature importance can be considered as a regression coefficient indicating how much a given variable contributes towards the CH_4 or N_2O bias-correction prediction. Variance and feature importances for SHmid, tropics, NHmid and NHpol are shown in Supplementary Figures S1 to S4, respectively. For SHpol, XGBoost seems to show excellent performance for both species throughout the stratosphere with R^2 values ranging from 0.6 to 0.8. This also validates our approach of using different long-lived tracers as variables in the regression model. As expected, concentrations of long-lived tracers seem to show close relationships to the biases seen in CH_4 and N_2O profiles. However, supplementary Figures S1 to S4 show that R^2 for other latitude bins are somewhat smaller (near 0.5) indicating regions with less dynamical variability (e.g. mid-latitudes) might need some additional features that are not included in this set up.

Another important aspect is that R^2 for CH_4 remain almost flat between 25 to 50 km, but for N_2O, R^2 values are close to 0.6 in the lower stratosphere and lower mesosphere with minima near 30 km. The time term (date) term is included in the XGBoost model to allow it to extrapolate corrections to data that lies outside the training period. However, in current setup, the feature importance of the time term is only significant at a few levels for some latitude bands (Figure 1 and Supplementary Figures S1 to S4). This suggests that the time term is not playing a major role in the model's predictions for these latitude bands. To improve model's performance, we also tried to increase number of trees, use Huber/quantile loss functions, but none of the changes helped to improve time term's significance. We have added discussion in a revised manuscript. In summary, in a current setup time (date) term is not very significant.

In Figure 1, dynamical variables such as potential vorticity ~~show the largest feature (variable) importance~~ are most important in explaining the biases in the lower stratosphere (near 18 ~~km)where~~ km). This is likely due to the fact that the TOMCAT model overestimates the fast isentropic transport ~~seems to be somewhat overestimated in the TOMCAT setup. It is also~~ in the lower stratosphere. However, it is important to note that the 50°S-90°S ~~covers a relatively~~ region covers a large part of the high-latitude stratosphere and includes the strong wintertime polar vortex as well as tracer variations near the edge of the vortex. ~~Hence attributing a single variable or a single processes~~ As a result, it is not possible to attribute the biases to a single variable or process. For example, ~~around 35 to 40 km, temperature variations seem to~~ temperature variations explain a large part of the CH_4 biases ~~but,~~ around 35 to 40 km, but $ClONO_2$ is most important just below 35 ~~kmthe $ClONO_2$ feature importance is largest (about 0.3)~~km. On the other hand, HNO_3 ~~seems to explain a large part of~~ is most important for explaining the N_2O biases in the mid-upper stratosphere. This ~~indicates thatalthough~~ suggests that, while there is a strong relationship between temperature~~potential vorticity~~ , potential vorticity, and chlorine activation, the biases in CH_4 and N_2O ~~biases in the stratosphere cannot be linked to a single process or~~ at a single level are generally better explained by a single variable.

For CH_4, additional features showing significant importances are water vapour, CH_4 and N_2O. As CH_4 is the largest in-situ source of stratospheric water vapour, their alternating importances in the lower mesosphere (above 55 km) indicate issues with HOx-related CH_4 loss in the lower mesosphere. On the other hand, in the lower stratosphere, a strong winter-time dehydration inside the polar vortex leads to significant drying. Hence, the somewhat larger importance for water vapour near 15 km and 23 km suggests that XGBoost is able to identify and attribute possible biases in TOMCAT setup to downward transport of CH_4 as well as the parameterised dehydration scheme. Similarly, the peaks in N_2O importance near the stratopause ($\sim$48km) and near 21 km indicate issues in the representation of the downward transport of the long-lived tracers from the mesosphere into the stratosphere in the polar vortex. Note that in our simulations the TOMCAT top model level is located near 60 km.

Next we compare vertical CH_4 profiles from TOMCAT, TCOM-CH4 and collocated HALOE/ACE for the SHpol latitude bin (Figure 2). Overall, we have have about 40,000 profiles of which around 30,000 fall in the XGBoost training period and about 10,000 profiles in the 2019-2021 evaluation period. Overall, TCOM-CH4 profiles show excellent agreement with satellite profiles and median lines seems to follow each other very closely. In contrast the TOMCAT profiles show good agreement with observational data between 20-30 km but exhibit positive biases at upper and lower levels. This distinct feature indicates a clear separation in the importance of dynamical and chemical processes controlling CH_4 concentrations. As mentioned earlier, positive biases in TOMCAT CH_4 in the lower stratosphere could be due to faster CH_4 transport from the tropics to high-latitudes. Positive biases in the upper stratosphere/lower mesosphere are most probably due to slower CH_4 loss via HOx and ClOx chemistry. Another important characteristic in Figure 2 is that variability in observational profiles (shaded region shows 10 and 90 percentiles) is much larger than TOMCAT (or TCOM) profiles. A possible explanation for differences in variability would be model output is sampled at the longitude/latitude recorded at 30 km tangent height, but in reality collocations at different altitudes are a few degrees apart. Additionally, the onion peeling algorithm used for solar occultation measurements assumes observations at different tangent height are independent, hence retrieved profiles show larger fluctuations.

Vertical profiles of the absolute (in ppm) and percentage (%) CH_4 differences between the three data sets are also shown in Figure 2 for both the training (1992-2018) and evaluation (2019-2021) time periods. As expected, the median TCOM-CH4

profiles show very little difference with respect to collocated median satellite profiles whereas the TOMCAT profile differences range from -0.22 ppm (16 km) to -0.05 (near 28 km). In terms of relative differences, again TCOM-observation differences are close to 0%, whereas for the evaluation period differences are up to 10% in the lower and middle stratosphere. A possible explanation for somewhat larger differences for 2019-2021 time period is that there has been rapid increase in atmospheric CH_4 over last few years (e.g. Nisbet et al., 2019). As the rapid CH_4 increase period is outside XGBoost training values, the estimated correction terms seem to be too small, but there are still significant improvements compared to TOMCAT profiles. Median profile comparisons for training and evaluation periods, and subsequent differences (in ppm and %) for other latitude bins, are shown in Supplementary Figures S5 to S8. And again, TCOM-observation comparison is consistent for other latitude bins as well, with an exception that mid-stratospheric biases for evaluation period are somewhat larger (up to 10%) for SH mid-lat and tropics (Figures s5 and S6).

Similarly for N_2O, Figure 3 compares median profiles from ACE-FTS N_2O, TCOM-N2O and TOMCAT and their differences (absolute and percentage) for SH polar latitudes. Again, TCOM-N2O and ACE-FTS profiles show excellent agreement for all stratospheric altitudes. Interestingly, TOMCAT N_2O profiles are high-biased only in the lower stratosphere (up to 25 km) and have negligible biases in the mid-upper stratosphere. So, in the lower stratosphere TOMCAT profiles show positive biases of up to ± 50 ppb, while TCOM-N2O biases are close to zero for the training period (2004–2010) but show a slight increase (up to ± 10 ppb) for the evaluation period (2019–2021). ~~Although~~ Some of these biases could be linked to the use of measurements with positive values only as well missing possible variable that would account for strong season variations at the higher latitudes in current set up to XGBoost. And, although TCOM-N2O biases are much smaller throughout the stratosphere, in percentage terms biases can reach up to 100% near 40 km as changes in the small values can translate into much larger changes in relative differences. However, even with those large relative differences, significantly reduced biases in TCOM-N2O profiles are visible for all the levels. Median profile comparisons and differences between ACE-FTS, TCOM-N2O, TOMCAT profiles (in ppb and %) for other latitude bins are shown in Supplementary Figures S9 to S12.

And similar to Figure 3, the absolute median differences between observed and TCOM values is less than 10 ppb. However, the relative differences in the upper stratosphere are much larger (up to 100%, especially in the SH midlat and tropics). This is likely due to the fact that TCOM only uses only positive values, which removes observations with low concentration profiles during the winter months.

Improvements in CH_4 and N_2O profiles are clearly visible in time series comparison shown in Figures 4 and 5 which compare CH_4 and N_2O evaluation at 20, 30, 40 and 50 km for the SHpol latitude bin. For clarity the figure shows every 10th profile (10% of data points). Similar comparisons for SHmid, tropics, NHmid and NHpol are shown in Supplementary Figures S13 to S20. TCOM-CH4 data points show excellent agreement with the HALOE and ACE data points (Figure 4). Uneven data density before and after 2004 reflect differences in viewing techniques between these two satellite instruments. Basically, HALOE was designed to provide near global coverage whereas ACE-FTS was designed to provide denser coverage at high latitudes. Even with these uneven sampling frequencies, we do not observe any abrupt changes in TCOM-CH4 data points. ~~However, we do note some unusual data points in 2004 in the HALOE data record but we are not sure of the exact causes of~~

these variations. An inspection of HALOE documentation (, last access: 10 November 2022) does not mention any outstanding issues regarding HALOE CH_4 retrievals.

Similarly for N_2O, Figure 5 also shows excellent agreement between TCOM-N2O and ACE-FTS data points. Again the largest corrections are observed in the lower stratosphere (15 to 25 km) where TOMCAT profiles are about 30 ppb high-biased that can be considered as systematic bias due to TOMCAT setup. Similar to CH_4, a seasonal minima occurs just after the break-up of Antarctic polar vortex (October) , transporting as descending branch of stratospheric circulation transports N_2O-depleted air to lower altitudes and latitudes (horizontal mixing). As N_2O mixing ratios decrease rapidly with increasing altitude, a large number of ACE-FTS data points show negligible N_2O values which is reflected in TCOM-N2O data points. However, it is also important to note that both CH_4 and N_2O mixing ratios decrease rapidly with increasing altitude (especially during SH winter/fall). As the ACE-FTS retrieval algorithm uses multiple micro-windows, there may be a seasonal shift in averaging kernels causing fluctuations in the retrieved profiles. We also find that the number of negative values in ACE-FTS data increase with increasing altitude. As a seasonal variation in vertical structure of the atmosphere alters spacing between tangent heights. Therefore, N_2O (as well as CH_4) profile variability increases when tangent heights get very close together. Additionally, as mixing ratio values get close to zero, retrieved profiles turn noisy as some values can be negative. Here, we use only positive data points for XGBoost training, correction terms used here might be influenced by these positively biased, influencing seasonal cycle effects in CH_4 and N_2O concentrations.

An important aspect seen in Figures 4 and 5 is that the seasonal cycles in TCOM-CH4 and TCOM-N2O data points seem to be more synchronised with observational data sets than TOMCAT, especially at 20 km. As shown above, TOMCAT profiles show positive biases throughout the stratosphere and largest corrections seem to be in the summertime maximum values that must arise from transport from mid-high latitudes. Interestingly, near 30 km points from all three data sets seem to be closer to each other for both CH_4 and N_2O. Finally, an interesting aspect in both Figures 4 and 5 is that in the upper stratosphere both species show wintertime minima near 40 to 50 km that are close to zero throughout the data record. Even with long-term trends in tropospheric concentrations, a casual inspection does not show any significant trends in either species. We aim to explore this aspect of CH_4 and N_2O trends in future studies.

Next we compare TCOM-CH4 profiles with the latest SPARC CH_4 data set Hegglin et al. (2021). Figure 6 show daily mean zonal mean CH_4 time series from TCOM-CH4 and monthly mean values from three SPARC (S-HALOE-CH4, S-MIPAS-CH4 and S-ACE-CH4) CH_4 data records. Unsurprisingly, with some exceptions (near 32.5°S and N), TCOM-CH4 shows best agreement with S-ACE-CH4 data at all pressure levels and latitude bins. At 50 hPa, TCOM-CH4 values show somewhat positive biases with respect to S-HALOE-CH4 near subtropical latitudes, but relatively better agreement in the middle (5 hPa) and upper (0.5 hPa) stratosphere. On the other hand, S-MIPAS-CH4 data points show significant positive biases with respect to all other data records with qualitative agreement in the upper stratosphere. Additionally, as expected, positive growth rates observed in the tropospheric CH_4 concentrations are also distinguishable in both observations (ACE + HALOE) and TCOM-CH4 data especially near tropical and subtropical latitudes at 50 hPa.

Figure 6 also compares the CH_4 evolution at 67.5° S and 67.5° N. As expected, wintertime CH_4 concentrations in the SH high latitudes are somewhat larger compared to the NH high-latitudes (e.g. Remsberg, 2015). This is because a stronger Brewer-

Dobson (BD) circulation in the NH causes faster downward propagation of the CH_4-poor air from the upper stratosphere to the lower-middle stratosphere. Interestingly, all the SPARC CH_4 data records show less CH_4 in the SH at 50 hPa than TCOM. At 5 hPa, TCOM-CH4 data show relatively better agreement with S-HALOE-CH4 data in both hemispheres and with S-ACE-CH4 data only in the NH. ~~The~~ Though exact causes of unusually low CH_4 values in S-MIPAS-CH4 and S-ACE-CH4 data files are unclear~~.~~, but might be associated with the downwards transport of CH_4 poor air (negative values in ACE/MIPAS retrieval) that are not used in XGBoost.It also suggests that winter-time downward descent at higher latitudes is somewhat weaker in TCOM data. Again, S-MIPAS-CH4 data points indicate a much larger magnitude of seasonal cycle compared to other data sets. In the upper stratosphere (0.5 hPa), there seems to better agreement among all the data in both hemispheres. Overall, we find that compared to the TCOM-CH4 data set, SPARC CH_4 data records have some inconsistent characteristics and largest disagreement is found to be at NH high latitudes.

Figure 7 compares the evolution of TCOM-N2O and SPARC data sets based on MIPAS, Aura-MLS, SMR and ACE measurements for five latitude grids (67.5°S, 32.5°S, 2.5°N, 32.5°N, and 67.5°N) and three pressure levels (50 hPa, 5 hPa, and 0.5 hPa). The lack of satellite measurements during the 1990s makes it difficult to compare the long-term N_2O evolution but significant differences between various satellite data records also complicate the more straightforward evaluation. Overall, TCOM-N2O shows best agreement with SPARC ACE-FTS (S-ACE-N2O) data and poorest agreement with SPARC MIPAS (S-MIPAS-N2O) data. Interestingly, SPARC SMR (S-SMR-N2O) show N_2O variations that are very similar to the S-MIPAS-N2O data set whereas SPARC-Aura-MLS (S-AMLS-N2O) agrees better with S-ACE-N2O with some exceptions in the later few years that are related to a drift in MLS N_2O measurement (190 GHz) channel (Livesey et al., 2021), especially in the lower stratosphere. Hence, for the earlier period TCOM-N2O also shows good agreement with S-AMLS-N2O data until 2014 and then slight drifts are distinguishable at low-mid latitudes. On the other hand, close agreement between S-SMR-N2O and S-MIPAS-N2O means that both data sets exhibit high biases in the lower stratosphere and again agreement is weakest at low-mid latitudes.

Another important aspect in Figure 7 is that at high latitudes, as well as for mid-upper stratospheric altitudes, all the SPARC data sets agree quite well with each other and there are no long-term drift and systematic biases between them. The good agreement of TCOM-N2O with all the SPARC N_2O data sets at 5 and 0.5 hPa provides additional evidence of the usefulness of the TCOM-N2O data set. Additionally, similar to TCOM-CH4, casual inspection of TCOM-N2O does not show any long-term trends at mid-upper stratospheric pressure levels; we aim to investigate this further in future studies.

Next we analyse differences between TCOM-CH4 and TOMCAT CH_4 profiles through the time evolution of corrections estimated by the XGBoost regression model. First we look at the differences in zonal mean CH_4 at different levels. Figure 8 shows TCOM-CH4 minus TOMCAT CH_4 differences (in %) at four vertical levels (15 to 45 km with 10 km spacing). An important aspect regarding 15 km and 25 km differences is that although median CH_4 differences shown in Figure 2 indicate TOMCAT profiles show positive biases (up to 10%), the latitude slice indicates significant variations between the two. Differences are even positive close to polar latitudes indicating stronger downward transport of CH_4-poor air and/or weaker mixing near the Antarctic polar vortex region in TOMCAT simulation. Similar characteristics are observed at NH high latitudes. These biases are even more distinctive at 25 km, especially in the SH high latitudes, though this region can be considered to be

a boundary region where dynamical processes control CH_4 concentration at lower altitude and chemical processes dominate at higher altitudes. Inter-hemispheric asymmetry in the CH_4 bias correction also indicates significant differences in representation of BD circulation in ERA5 data (e.g. Li et al., 2022).

Additionally, some uneven differences for 1991-1993 at 15 and 25 km in Figure 8 could be due to a combination of various chemical and dynamical processes. For example, volcanically enhanced stratospheric aerosol following the Mt. Pinatubo eruption in June 1991, might have altered stratospheric transport pathways as larger aerosols absorb outgoing long-wave radiation (Free and Lanzante, 2009; Dhomse et al., 2020). Such heating can also enhance tropical upwelling as well as horizontal mixing on isentropic surfaces (e.g. Poberaj et al., 2011; Dhomse et al., 2015; Bittner et al., 2016). Volcanically enhanced stratospheric aerosol can also alter OH radical concentrations either by modulating the amount of incoming solar radiation or by altering chemical pathways (e.g. Bândă et al., 2013, 2016). It is also well known that increases in stratospheric aerosol concentration also affected HALOE retrievals (e.g. Remsberg, 2008). ERA5 data assimilation does not include these atmospheric effects of volcanically enhanced stratospheric aerosol (e.g. Hersbach et al., 2020), hence we are not sure about the unusual CH_4 differences in the lower stratosphere.

On the other hand, differences at 35 km in Figure 8 seem to be dominated by the QBO-induced meridional circulation patterns Baldwin et al. (2001), that are underestimated in TOMCAT. Even though ACE provides limited observational data points in the tropics, XGBoost is able to identify this discrepancy. On the temporal scale, differences are largest until 1996, reaching polar latitudes, followed by gradual decrease in the NH sub-tropics and remain larger in the SH sub-tropics. A similar type of uneven evolution for later periods can also be seen, suggesting issues in ERA5 data towards the representation of QBO-induced circulation, especially for years with an unusual QBO evolution such as 2016 and 2020 (e.g. Newman et al., 2016; Osprey et al., 2016; Diallo et al., 2022).

Another notable feature in Figure 8 is that at 45 km, for some years CH_4 differences are clearly distinguishable. Both HALOE and ACE have much smaller retrieval errors at higher altitude and, assuming there were no abrupt changes in these two satellite instruments (or retrieval algorithms), the unusual differences seen at 45 km can be attributed to inhomogeneities or issues in ERA5 data. These distinctive periods include the first halves of years 1993, 1997, 2001, 2004 and the latter half of 2019.

6 Summary and Conclusions

Even though CH_4 and N_2O are very important greenhouse gases, as well as the sources for key stratospheric species, there are limited stratospheric profile data sets that extend for more than a decade. Due to their long lifetimes, CH_4 and N_2O are also very useful dynamical tracers, that can used to evaluate stratospheric transport processes. Also, for the accurate retrieval of tropospheric CH_4 using satellite instruments, realistic stratospheric CH_4 profiles provide a useful constraint. However, until now no attempt has been made to construct long-term CH_4 and N_2O profile data sets. Furthermore, although chemical models are able to simulate long-term profile data sets of these species, they are highly dependent on the dynamical scheme used to simulate stratospheric transport processes as well as chemical loss rates/processes used in a particular model.

Here we have used CH_4 and N_2O profiles from the TOMCAT CTM, two solar occultation instrument measurements and the eXtreme Gradient Boost (XGBoost) regression model to construct daily, gap-free stratospheric profile data sets (TCOM-CH4 and TCOM-N2O) for the 1991-2021 time period. The XGBoost regression model is trained for the CH_4 or N_2O difference between TOMCAT and satellite measurements (HALOE and ACE). These differences are used to estimate corrections that are added to the TOMCAT profiles to derive TCOM-CH4 and TCOM-N2O profiles. The regression algorithm uses 13 features (or variables) based on TOMCAT tracers as well as four additional features such as temperature, potential vorticity, latitude and date of the measurement. As atmospheric CH_4 and N_2O concentrations vary under different dynamical and chemical regimes, the global measurements are sub-divided in five latitude bins (two polar, two mid-latitude and the tropics) within which regression parameters are derived for each 1 km vertical grid (15 to 60 km).

For both the gases, XGBoost shows good performance (R^2 >0.5 to 0.8) throughout the stratosphere, except for lower stratosphere which can be attributed to the limited training measurements. Measurements from the final three years (2019-2021) are used evaluate TCOM-CH4 and TCOM-N2O profiles. Overall, TCOM-CH4 show excellent agreement with the evaluation profiles and median differences are less than 10%. Additionally, comparison with SPARC-CH4 data suggests that SPARC-MIPAS profiles show some unrealistic behaviour and SPARC-ACE and SPARC-HALOE do not show expected inter-hemispheric differences in lower stratospheric CH_4 differences (less CH_4 in the NH).

For TCOM-N2O, better agreement is again seen with respect to S-ACE-N2O data set and weaker agreement is observed against MIPAS data. TCOM-N2O also confirms the drift in Aura-MLS (as used in SPARC data set) especially at lower latitudes and altitudes. A simple inspection of TCOM-CH4 and TCOM-N2O plots also suggests that despite increasing surface values there are near-negligible long-term trends in the upper stratosphere/lower mesosphere which is consistent with Minganti et al. (2022). A possible explanation would be ~~strengthening of~~ stratospheric/mesospheric loss processes probably determined by changes in the stratospheric circulation ~~which would have caused faster photochemical loss thereby~~ is reducing the lifetime of these GHGs (e.g. Prather et al., 2022), thereby compensating enhancement in the tropical entry mixing ratio due to increasing tropospheric emissions. Finally, analysis of TCOM-CH4 and TOMCAT CH4 profiles suggests that the representation of QBO-induced secondary circulation is not adequate in the CTM and differences also reveal some temporal inhomogeneities in ERA5 reanalysis data.

Presently, the TCOM-CH4 and TCOM-N2O V1.0 data set is ideally suited for the evaluation of CH_4 and N_2O chemistry and stratospheric transport processes in models. The TCOM-CH4 data set can also be used as realistic stratospheric profiles in a CH_4 profile/total column retrievals. Daily mean zonal mean TCOM-CH4 and TCOM-N2O profile data on pressure and altitude levels in mixing ratio units are publicly available via https://doi.org/10.5281/zenodo.7293740 (Dhomse, 2022a) and https://doi.org/10.5281/zenodo.7386001 (Dhomse, 2022b), respectively.

7 Data availability

HALOE V19 are from https://acdisc.gesdisc.eosdis.nasa.gov/data//UARS_HALOE_Level2/, ACE-FTS v4.2 is obtained via http://www.ace.uwaterloo.ca/data.php. SPARC climatological data can be obtained via doi:10.5281/zenodo.4265393 (Hegglin

et al., 2021). TCOM-CH4 and TCO-N2O data are publicly available at https://doi.org/10.5281/zenodo.7293740 (Dhomse, 2022a) and https://doi.org/10.5281/zenodo.7386001 (Dhomse, 2022b), respectively.

Author contributions. SSD conceived and designed the study. MPC performed TOMCAT model simulations. SSD performed the analysis. SSD and MPC co-wrote the paper

Competing interests. Authors declare no conflicts of interests.

Acknowledgements. This work was supported by the NERC SISLAC (NE/R001782/1) and LSO3 (NE/V0011863/1) projects. We thank HALOE and ACE-FTS science teams for the data sets. We thank the European Centre for Medium-Range Weather Forecasts for providing their analyses. TOMCAT simulations were performed on the UK national Archer and Leeds Arc4 HPC systems.

References

Arosio, C., Rozanov, A., Malinina, E., Eichmann, K.-U., von Clarmann, T., and Burrows, J. P.: Retrieval of ozone profiles from OMPS limb scattering observations, Atmospheric Measurement Techniques, 11, 2135–2149, https://doi.org/10.5194/amt-11-2135-2018, 2018.

Baldwin, M. P., Gray, L. J., Dunkerton, T. J., Hamilton, K., Haynes, P. H., Randel, W. J., Holton, J. R., Alexander, M. J., Hirota, I., Horinouchi, T., Jones, D. B. A., Kinnersley, J. S., Marquardt, C., Sato, K., and Takahashi, M.: The quasi-biennial oscillation, Reviews of Geophysics, 39, 179–229, https://doi.org/10.1029/1999RG000073, 2001.

Bândă, N., Krol, M., van Weele, M., van Noije, T., and Röckmann, T.: Analysis of global methane changes after the 1991 Pinatubo volcanic eruption, Atmospheric Chemistry and Physics, 13, 2267–2281, https://doi.org/10.5194/acp-13-2267-2013, 2013.

Bândă, N., Krol, M., van Weele, M., van Noije, T., Le Sager, P., and Röckmann, T.: Can we explain the observed methane variability after the Mount Pinatubo eruption?, Atmospheric Chemistry and Physics, 16, 195–214, https://doi.org/10.5194/acp-16-195-2016, 2016.

Bernath, P.: Atmospheric Chemistry Experiment (ACE): An overview, IEEE International Geoscience and Remote Sensing Symposium, 2, 147–160, http://eprints.whiterose.ac.uk/68898/, 2002.

Bernath, P. F., McElroy, C. T., Abrams, M. C., Boone, C. D., Butler, M., Camy-Peyret, C., Carleer, M., Clerbaux, C., Coheur, P.-F., Colin, R., DeCola, P., DeMazière, M., Drummond, J. R., Dufour, D., Evans, W. F. J., Fast, H., Fussen, D., Gilbert, K., Jennings, D. E., Llewellyn, E. J., Lowe, R. P., Mahieu, E., McConnell, J. C., McHugh, M., McLeod, S. D., Michaud, R., Midwinter, C., Nassar, R., Nichitiu, F., Nowlan, C., Rinsland, C. P., Rochon, Y. J., Rowlands, N., Semeniuk, K., Simon, P., Skelton, R., Sloan, J. J., Soucy, M.-A., Strong, K., Tremblay, P., Turnbull, D., Walker, K. A., Walkty, I., Wardle, D. A., Wehrle, V., Zander, R., and Zou, J.: Atmospheric Chemistry Experiment (ACE): Mission overview, Geophysical Research Letters, 32, https://doi.org/https://doi.org/10.1029/2005GL022386, 2005.

Bittner, M., Schmidt, H., Timmreck, C., and Sienz, F.: Using a large ensemble of simulations to assess the Northern Hemisphere stratospheric dynamical response to tropical volcanic eruptions and its uncertainty, Geophysical Research Letters, 43, 9324–9332, https://doi.org/10.1002/2016GL070587, 2016.

Boone, C., Bernath, P., Cok, D., Jones, S., and Steffen, J.: Version 4 retrievals for the atmospheric chemistry experiment Fourier transform spectrometer (ACE-FTS) and imagers, Journal of Quantitative Spectroscopy and Radiative Transfer, 247, 106 939, https://doi.org/https://doi.org/10.1016/j.jqsrt.2020.106939, 2020.

Chen, T. and Guestrin, C.: Xgboost: A scalable tree boosting system, in: Proceedings of the 22nd acm sigkdd international conference on knowledge discovery and data mining, pp. 785–794, 2016.

Chipperfield, M., Liang, Q., Abraham, L., Bekki, S., Braesicke, P., Dhomse, S., Genova, G. D., Fleming, E., Hardiman, S. C., Iachettii, D., Jackman, C. H., Kinnison, D. E., Marchand, M., Pitari, G., Rozanov, E., Stenke, A., and Tummon, F.: Lifetimes of Stratospheric Ozone-Depleting Substances, Their Replacements, and Related Species, Tech. rep., SPARC, http://www.sparc-climate.org/fileadmin/customer/6{_}Publications/SPARC{_}reports{_}PDF/6{_}LifetimeReport{_}Ch5.pdfhttp://www.sparc-climate.org/publications/sparc-reports/sparc-report-no6/, 2013.

Chipperfield, M. P.: New version of the TOMCAT/SLIMCAT off-line chemical transport model: Intercomparison of stratospheric tracer experiments, Quarterly Journal of the Royal Meteorological Society, 132, 1179–1203, https://doi.org/10.1256/qj.05.51, 2006.

Davis, S. M., Rosenlof, K. H., Hassler, B., Hurst, D. F., Read, W. G., Vömel, H., Selkirk, H., Fujiwara, M., and Damadeo, R.: The Stratospheric Water and Ozone Satellite Homogenized (SWOOSH) database: a long-term database for climate studies, Earth System Science Data, 8, 461–490, https://doi.org/10.5194/essd-8-461-2016, 2016.

Dhomse, S.: TCOM-CH4: TOMCAT CTM and Occultation Measurements based daily zonal stratospheric methane profile dataset [1991-2021] constructed using machine- learning, https://doi.org/10.5281/zenodo.7293740, 2022a.

Dhomse, S.: TCOM-N2O: TOMCAT CTM and Occultation Measurements based daily zonal stratospheric nitrous oxide profile dataset [1991-2021] constructed using machine-learning, https://doi.org/10.5281/zenodo.7386001, 2022b.

Dhomse, S. S., Chipperfield, M. P., Feng, W., Hossaini, R., Mann, G. W., and Santee, M. L.: Revisiting the hemispheric asymmetry in midlatitude ozone changes following the Mount Pinatubo eruption: A 3-D model study, Geophysical Research Letters, 42, 3038–3047, https://doi.org/10.1002/2015GL063052, 2015.

Dhomse, S. S., Chipperfield, M. P., Damadeo, R. P., Zawodny, J. M., Ball, W. T., Feng, W., Hossaini, R., Mann, G. W., and Haigh, J. D.: On the ambiguous nature of the 11-year solar cycle signal in upper stratospheric ozone, Geophysical Research Letters, 43, 7241–7249, https://doi.org/10.1002/2016GL069958, 2016.

Dhomse, S. S., Mann, G. W., Antuña Marrero, J. C., Shallcross, S. E., Chipperfield, M. P., Carslaw, K. S., Marshall, L., Abraham, N. L., and Johnson, C. E.: Evaluating the simulated radiative forcings, aerosol properties, and stratospheric warmings from the 1963 Mt Agung, 1982 El Chichón, and 1991 Mt Pinatubo volcanic aerosol clouds, Atmospheric Chemistry and Physics, 20, 13 627–13 654, https://doi.org/10.5194/acp-20-13627-2020, 2020.

Dhomse, S. S., Arosio, C., Feng, W., Rozanov, A., Weber, M., and Chipperfield, M. P.: ML-TOMCAT: machine-learning-based satellite-corrected global stratospheric ozone profile data set from a chemical transport model, Earth System Science Data, 13, 5711–5729, https://doi.org/10.5194/essd-13-5711-2021, 2021.

Dhomse, S. S., Chipperfield, M. P., Feng, W., Hossaini, R., Mann, G. W., Santee, M. L., and Weber, M.: A single-peak-structured solar cycle signal in stratospheric ozone based on Microwave Limb Sounder observations and model simulations, Atmospheric Chemistry and Physics, 22, 903–916, 2022.

Diallo, M. A., Ploeger, F., Hegglin, M. I., Ern, M., Grooß, J.-U., Khaykin, S., and Riese, M.: Stratospheric water vapour and ozone response to the quasi-biennial oscillation disruptions in 2016 and 2020, Atmospheric Chemistry and Physics, 22, 14 303–14 321, https://doi.org/10.5194/acp-22-14303-2022, 2022.

Drummond, J., Houghton, J. T., Peskett, G., Rodgers, C., Wale, M., Whitney, J., and Williamson, E.: The stratospheric and mesospheric sounder on Nimbus 7, Philosophical Transactions of the Royal Society of London. Series A, Mathematical and Physical Sciences, 296, 219–241, 1980.

Farman, J. C., Gardiner, B. G., and Shanklin, J. D.: Large losses of total ozone in Antarctica reveal seasonal ClO x/NO x interaction, Nature, 315, 207–210, 1985.

Free, M. and Lanzante, J.: Effect of Volcanic Eruptions on the Vertical Temperature Profile in Radiosonde Data and Climate Models, Journal of Climate, 22, 2925–2939, https://doi.org/10.1175/2008JCLI2562.1, 2009.

Gunson, M., Farmer, C. B., Norton, R., Zander, R., Rinsland, C. P., Shaw, J., and Gao, B.-C.: Measurements of CH4, N2O, CO, H2O, and O3 in the middle atmosphere by the Atmospheric Trace Molecule Spectroscopy Experiment on Spacelab 3, Journal of Geophysical Research: Atmospheres, 95, 13 867–13 882, 1990.

Hassler, B., Bodeker, G., and Dameris, M.: A new global database of trace gases and aerosols from multiple sources of high vertical resolution measurements, Atmospheric Chemistry and Physics, 8, 5403–5421, 2008.

Hassler, B., Kremser, S., Bodeker, G. E., Lewis, J., Nesbit, K., Davis, S. M., Chipperfield, M. P., Dhomse, S. S., and Dameris, M.: An updated version of a gap-free monthly mean zonal mean ozone database, Earth System Science Data, 10, 1473–1490, 2018.

Hegglin, M. I., Tegtmeier, S., Anderson, J., Bourassa, A. E., Brohede, S., Degenstein, D., Froidevaux, L., Funke, B., Gille, J., Kasai, Y., Kyrölä, E., Lumpe, J., Murtagh, D., Neu, J. L., Pérot, K., Remsberg, E., Rozanov, A., Toohey, M., von Clarmann, T., Walker, K. A., Wang, H. J., Damadeo, R., Fuller, R., Lingenfelser, G., Roth, C., Ryan, N. J., Sioris, C., Smith, L., and Weigel, K.: SPARC Data Initiative monthly zonal mean composition measurements from stratospheric limb sounders (1978-2018), https://doi.org/10.5281/zenodo.4265393, 2020.

Hegglin, M. I., Tegtmeier, S., Anderson, J., Bourassa, A. E., Brohede, S., Degenstein, D., Froidevaux, L., Funke, B., Gille, J., Kasai, Y., Kyrölä, E. T., Lumpe, J., Murtagh, D., Neu, J. L., Pérot, K., Remsberg, E. E., Rozanov, A., Toohey, M., Urban, J., von Clarmann, T., Walker, K. A., Wang, H.-J., Arosio, C., Damadeo, R., Fuller, R. A., Lingenfelser, G., McLinden, C., Pendlebury, D., Roth, C., Ryan, N. J., Sioris, C., Smith, L., and Weigel, K.: Overview and update of the SPARC Data Initiative: comparison of stratospheric composition measurements from satellite limb sounders, Earth System Science Data, 13, 1855–1903, https://doi.org/10.5194/essd-13-1855-2021, 2021.

Hersbach, H., Bell, B., Berrisford, P., Hirahara, S., Horányi, A., Muñoz-Sabater, J., Nicolas, J., Peubey, C., Radu, R., Schepers, D., Simmons, A., Soci, C., Abdalla, S., Abellan, X., Balsamo, G., Bechtold, P., Biavati, G., Bidlot, J., Bonavita, M., De Chiara, G., Dahlgren, P., Dee, D., Diamantakis, M., Dragani, R., Flemming, J., Forbes, R., Fuentes, M., Geer, A., Haimberger, L., Healy, S., Hogan, R. J., Hólm, E., Janisková, M., Keeley, S., Laloyaux, P., Lopez, P., Lupu, C., Radnoti, G., de Rosnay, P., Rozum, I., Vamborg, F., Villaume, S., and Thépaut, J.-N.: The ERA5 global reanalysis, Quarterly Journal of the Royal Meteorological Society, 146, 1999–2049, https://doi.org/https://doi.org/10.1002/qj.3803, 2020.

Inness, A., Blechschmidt, A.-M., Bouarar, I., Chabrillat, S., Crepulja, M., Engelen, R. J., Eskes, H., Flemming, J., Gaudel, A., Hendrick, F., Huijnen, V., Jones, L., Kapsomenakis, J., Katragkou, E., Keppens, A., Langerock, B., de Mazière, M., Melas, D., Parrington, M., Peuch, V. H., Razinger, M., Richter, A., Schultz, M. G., Suttie, M., Thouret, V., Vrekoussis, M., Wagner, A., and Zerefos, C.: Data assimilation of satellite-retrieved ozone, carbon monoxide and nitrogen dioxide with ECMWF's Composition-IFS, Atmospheric Chemistry and Physics, 15, 5275–5303, https://doi.org/10.5194/acp-15-5275-2015, 2015.

Jones, R. and Pyle, J.: Observations of CH4 and N2O by the Nimbus 7 SAMS: A comparison with in situ data and two-dimensional numerical model calculations, Journal of Geophysical Research: Atmospheres, 89, 5263–5279, 1984.

Lan, X., Nisbet, E. G., Dlugokencky, E. J., and Michel, S. E.: What do we know about the global methane budget? Results from four decades of atmospheric CH₄ observations and the way forward, Philosophical Transactions of the Royal Society A: Mathematical, Physical and Engineering Sciences, 379, 20200 440, https://doi.org/10.1098/rsta.2020.0440, 2021.

Lelieveld, J., Crutzen, P. J., and Dentener, F. J.: Changing concentration, lifetime and climate forcing of atmospheric methane, Tellus B, 50, 128–150, 1998.

Li, Y., Dhomse, S. S., Chipperfield, M. P., Feng, W., Chrysanthou, A., Xia, Y., and Guo, D.: Effects of reanalysis forcing fields on ozone trends and age of air from a chemical transport model, Atmospheric Chemistry and Physics, 22, 10 635–10 656, https://doi.org/10.5194/acp-22-10635-2022, 2022.

Livesey, N. J., Read, W. G., Froidevaux, L., Lambert, A., Santee, M. L., Schwartz, M. J., Millán, L. F., Jarnot, R. F., Wagner, P. A., Hurst, D. F., Walker, K. A., Sheese, P. E., and Nedoluha, G. E.: Investigation and amelioration of long-term instrumental drifts in water vapor and nitrous oxide measurements from the Aura Microwave Limb Sounder (MLS) and their implications for studies of variability and trends, Atmospheric Chemistry and Physics, 21, 15 409–15 430, https://doi.org/10.5194/acp-21-15409-2021, 2021.

Meinshausen, M., Nicholls, Z. R. J., Lewis, J., Gidden, M. J., Vogel, E., Freund, M., Beyerle, U., Gessner, C., Nauels, A., Bauer, N., Canadell, J. G., Daniel, J. S., John, A., Krummel, P. B., Luderer, G., Meinshausen, N., Montzka, S. A., Rayner, P. J., Reimann, S., Smith, S. J., van den

Berg, M., Velders, G. J. M., Vollmer, M. K., and Wang, R. H. J.: The shared socio-economic pathway (SSP) greenhouse gas concentrations and their extensions to 2500, Geoscientific Model Development, 13, 3571–3605, https://doi.org/10.5194/gmd-13-3571-2020, 2020.

Minganti, D., Chabrillat, S., Errera, Q., Prignon, M., Kinnison, D. E., Garcia, R. R., Abalos, M., Alsing, J., Schneider, M., Smale, D., Jones, N., and Mahieu, E.: Evaluation of the N2O Rate of Change to Understand the Stratospheric Brewer-Dobson Circulation in a Chemistry-Climate Model, Journal of Geophysical Research: Atmospheres, 127, e2021JD036 390, https://doi.org/https://doi.org/10.1029/2021JD036390, e2021JD036390 2021JD036390, 2022.

Newman, P., Coy, L., Pawson, S., and Lait, L.: The anomalous change in the QBO in 2015–2016, Geophysical Research Letters, 43, 8791–8797, 2016.

Nisbet, E. G., Manning, M., Dlugokencky, E., Fisher, R., Lowry, D., Michel, S., Myhre, C. L., Platt, S. M., Allen, G., Bousquet, P., et al.: Very strong atmospheric methane growth in the 4 years 2014–2017: Implications for the Paris Agreement, Global Biogeochemical Cycles, 33, 318–342, 2019.

Noël, S., Bramstedt, K., Hilker, M., Liebing, P., Plieninger, J., Reuter, M., Rozanov, A., Sioris, C. E., Bovensmann, H., and Burrows, J. P.: Stratospheric CH_4 and CO_2 profiles derived from SCIAMACHY solar occultation measurements, Atmospheric Measurement Techniques, 9, 1485–1503, 2016.

Noël, S., Weigel, K., Bramstedt, K., Rozanov, A., Weber, M., Bovensmann, H., and Burrows, J. P.: Water vapour and methane coupling in the stratosphere observed using SCIAMACHY solar occultation measurements, Atmospheric Chemistry and Physics, 18, 4463–4476, 2018.

Osprey, S. M., Butchart, N., Knight, J. R., Scaife, A. A., Hamilton, K., Anstey, J. A., Schenzinger, V., and Zhang, C.: An unexpected disruption of the atmospheric quasi-biennial oscillation, Science, https://doi.org/10.1126/science.aah4156, 2016.

Poberaj, C. S., Staehelin, J., and Brunner, D.: Missing Stratospheric Ozone Decrease at Southern Hemisphere Middle Latitudes after Mt. Pinatubo: A Dynamical Perspective, Journal of the Atmospheric Sciences, 68, 1922–1945, https://doi.org/10.1175/JAS-D-10-05004.1, 2011.

Prather, M. J., Froidevaux, L., and Livesey, N. J.: Observed changes in stratospheric circulation: Decreasing lifetime of N_2O, 2005–2021, Atmospheric Chemistry and Physics Discussions, 2022, 1–13, https://doi.org/10.5194/acp-2022-650, 2022.

Randel, W. J. and Wu, F.: A stratospheric ozone profile data set for 1979–2005: Variability, trends, and comparisons with column ozone data, Journal of Geophysical Research: Atmospheres, 112, 2007.

Remedios, J., Ruth, S., Rodgers, C., Taylor, F., Roche, A., Gille, J., Gunson, M., Russell III, J., Park, J., and Zipf, E.: Measurements of methane and nitrous oxide distributions by the improved stratospheric and mesospheric sounder: Retrieval and validation, Journal of Geophysical Research: Atmospheres, 101, 9843–9871, 1996.

Remsberg, E.: On the response of Halogen Occultation Experiment (HALOE) stratospheric ozone and temperature to the 11-year solar cycle forcing, Journal of Geophysical Research: Atmospheres . . . , http://onlinelibrary.wiley.com/doi/10.1029/2008JD010189/full, 2008.

Remsberg, E. E.: Methane as a diagnostic tracer of changes in the Brewer–Dobson circulation of the stratosphere, Atmospheric Chemistry and Physics, 15, 3739–3754, https://doi.org/10.5194/acp-15-3739-2015, 2015.

Russell III, J. M., Gordley, L. L., Park, J. H., Drayson, S. R., Hesketh, W. D., Cicerone, R. J., Tuck, A. F., Frederick, J. E., Harries, J. E., and Crutzen, P. J.: The halogen occultation experiment, Journal of Geophysical Research: Atmospheres, 98, 10 777–10 797, 1993.

Saunois, M., Bousquet, P., Poulter, B., Peregon, A., Ciais, P., Canadell, J. G., Dlugokencky, E. J., Etiope, G., Bastviken, D., Houweling, S., et al.: The global methane budget 2000–2012, Earth System Science Data, 8, 697–751, 2016.

Strong, K., Wolff, M. A., Kerzenmacher, T. E., Walker, K. A., Bernath, P. F., Blumenstock, T., Boone, C., Catoire, V., Coffey, M., De Mazière, M., Demoulin, P., Duchatelet, P., Dupuy, E., Hannigan, J., Höpfner, M., Glatthor, N., Griffith, D. W. T., Jin, J. J., Jones, N., Jucks, K.,

Kuellmann, H., Kuttippurath, J., Lambert, A., Mahieu, E., McConnell, J. C., Mellqvist, J., Mikuteit, S., Murtagh, D. P., Notholt, J., Piccolo, C., Raspollini, P., Ridolfi, M., Robert, C., Schneider, M., Schrems, O., Semeniuk, K., Senten, C., Stiller, G. P., Strandberg, A., Taylor, J., Tétard, C., Toohey, M., Urban, J., Warneke, T., and Wood, S.: Validation of ACE-FTS N_2O measurements, Atmospheric Chemistry and Physics, 8, 4759–4786, https://doi.org/10.5194/acp-8-4759-2008, 2008.

Tian, H., Xu, R., Canadell, J. G., Thompson, R. L., Winiwarter, W., Suntharalingam, P., Davidson, E. A., Ciais, P., Jackson, R. B., Janssens-Maenhout, G., Prather, M. J., Regnier, P., Pan, N., Pan, S., Peters, G. P., Shi, H., Tubiello, F. N., Zaehle, S., Zhou, F., Arneth, A., Battaglia, G., Berthet, S., Bopp, L., Bouwman, A. F., Buitenhuis, E. T., Chang, J., Chipperfield, M. P., Dangal, S. R. S., Dlugokencky, E., Elkins, J. W., Eyre, B. D., Fu, B., Hall, B., Ito, A., Joos, F., Krummel, P. B., Landolfi, A., Laruelle, G. G., Lauerwald, R., Li, W., Lienert, S., Maavara, T., MacLeod, M., Millet, D. B., Olin, S., Patra, P. K., Prinn, R. G., Raymond, P. A., Ruiz, D. J., van der Werf, G. R., Vuichard, N., Wang, J., Weiss, R. F., Wells, K. C., Wilson, C., Yang, J., and Yao, Y.: A comprehensive quantification of global nitrous oxide sources and sinks, Nature, 586, 248–256, 2020.

Urban, J., Lautié, N., Le Flochmoën, E., Jiménez, C., Eriksson, P., de La Noë, J., Dupuy, E., El Amraoui, L., Frisk, U., Jégou, F., Murtagh, D., Olberg, M., Ricaud, P., Camy-Peyret, C., Dufour, G., Payan, S., Huret, N., Pirre, M., Robinson, A. D., Harris, N. R. P., Bremer, H., Kleinböhl, A., Küllmann, K., Künzi, K., Kuttippurath, J., Ejiri, M. K., Nakajima, H., Sasano, Y., Sugita, T., Yokota, T., Piccolo, C., Raspollini, P., and Ridolfi, M.: Odin/SMR limb observations of stratospheric trace gases: Validation of N2O, Journal of Geophysical Research: Atmospheres, 110, https://doi.org/https://doi.org/10.1029/2004JD005394, 2005.

Waters, J. W., Froidevaux, L., Harwood, R. S., Jarnot, R. F., Pickett, H. M., Read, W. G., Siegel, P. H., Cofield, R. E., Filipiak, M. J., Flower, D. A., et al.: The earth observing system microwave limb sounder (EOS MLS) on the Aura satellite, IEEE transactions on geoscience and remote sensing, 44, 1075–1092, 2006.

WMO: Scientific Assessment of Ozone Depletion:2018, Tech. rep., World Meteorological Organization, Global Ozone Research and Monitoring Project, Report No. 58, Geneva, Switzerland, https://www.wmo.int/pages/prog/arep/gaw/ozone{_}2018/, 2018.

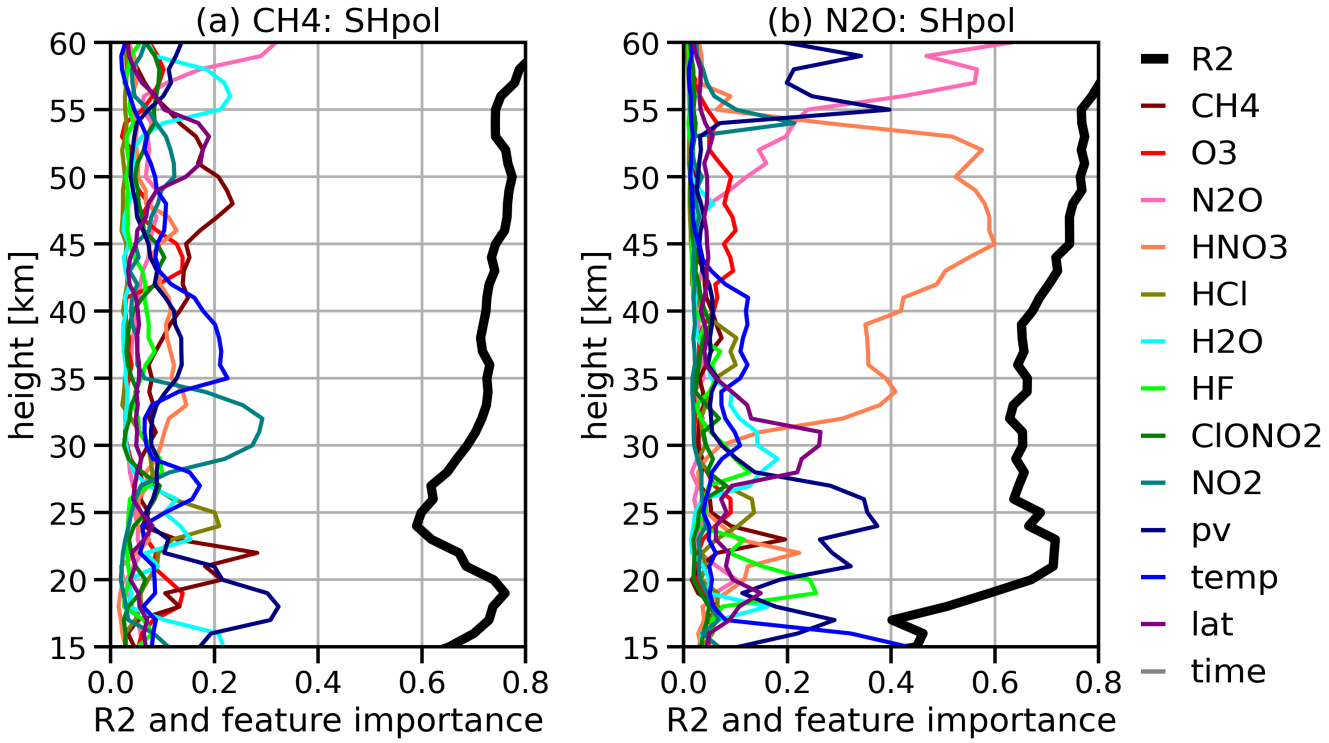

Figure 1. Vertical profiles of the variance (R^2) and feature importances estimated by XGBoost regression models for the TOMCAT-observation differences for (a) CH_4 (1991-2018) and (b) N_2O (2004-2018, ACE only) for the SHpol (50°S–90°S) latitude bin. See equation 1 and subsequent information about the features (total 13) or variables used in the XGBoost regression model.

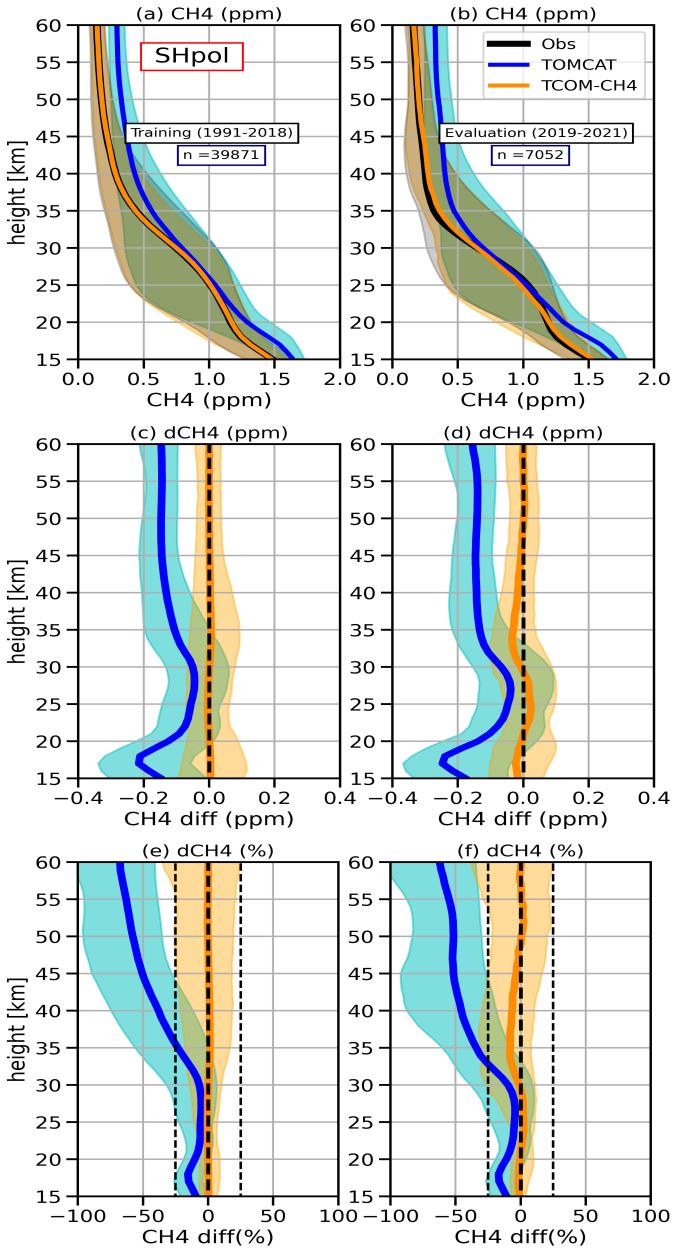

Figure 2. Panels (a) and (b). Comparison between TOMCAT (blue), TCOM-CH4 (orange) and satellite measurement-based (black) CH_4 profiles for SHpol (50°S–90°S) latitude band. Solid lines indicate median profiles while shaded regions show 10th and 90th percentile range. Comparisons are shown for training (1992-2018) and evaluation (2019-2021) periods in panels (a, left) and (b, right), respectively. Panels (c) - (f). Differences between TOMCAT and TCOM-CH4 w. r. t. satellite data sets in absolute units (ppm) and percent. Right (c and e) and left (d and f) panels show differences for the training (1992-2018) and evaluation (2019-2021) periods.

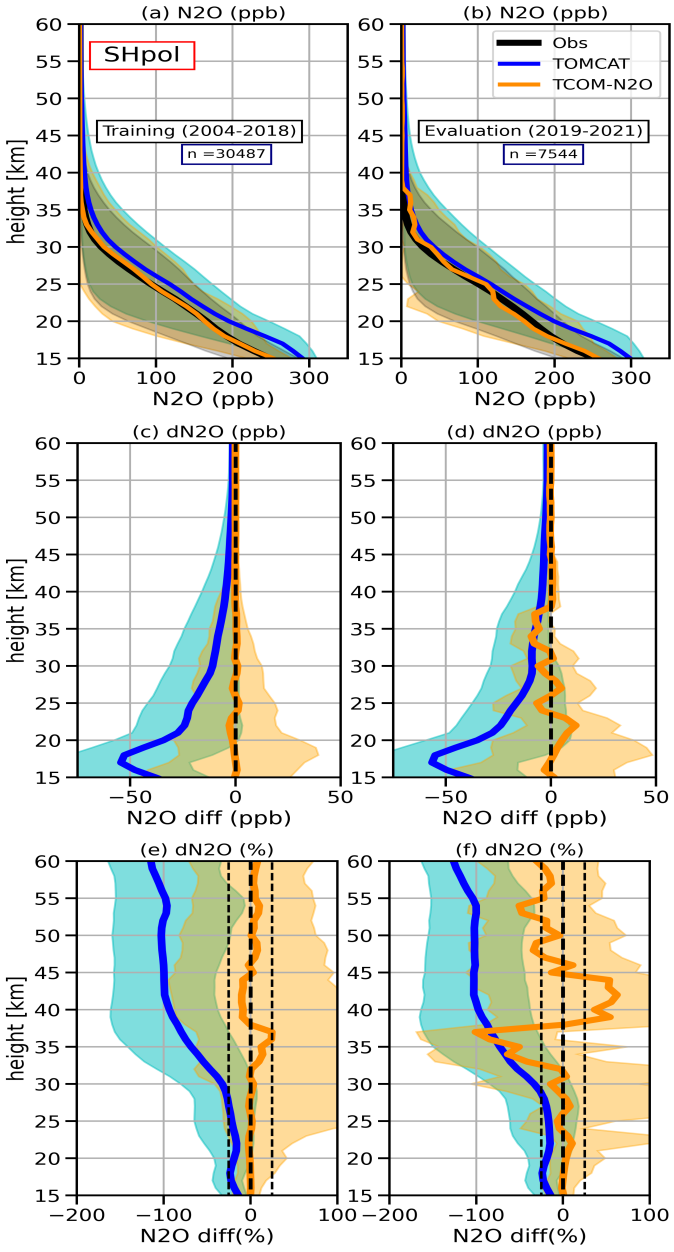

Figure 3. Same as Figure 2, but for N_2O. The training period includes data for 2004–2018.

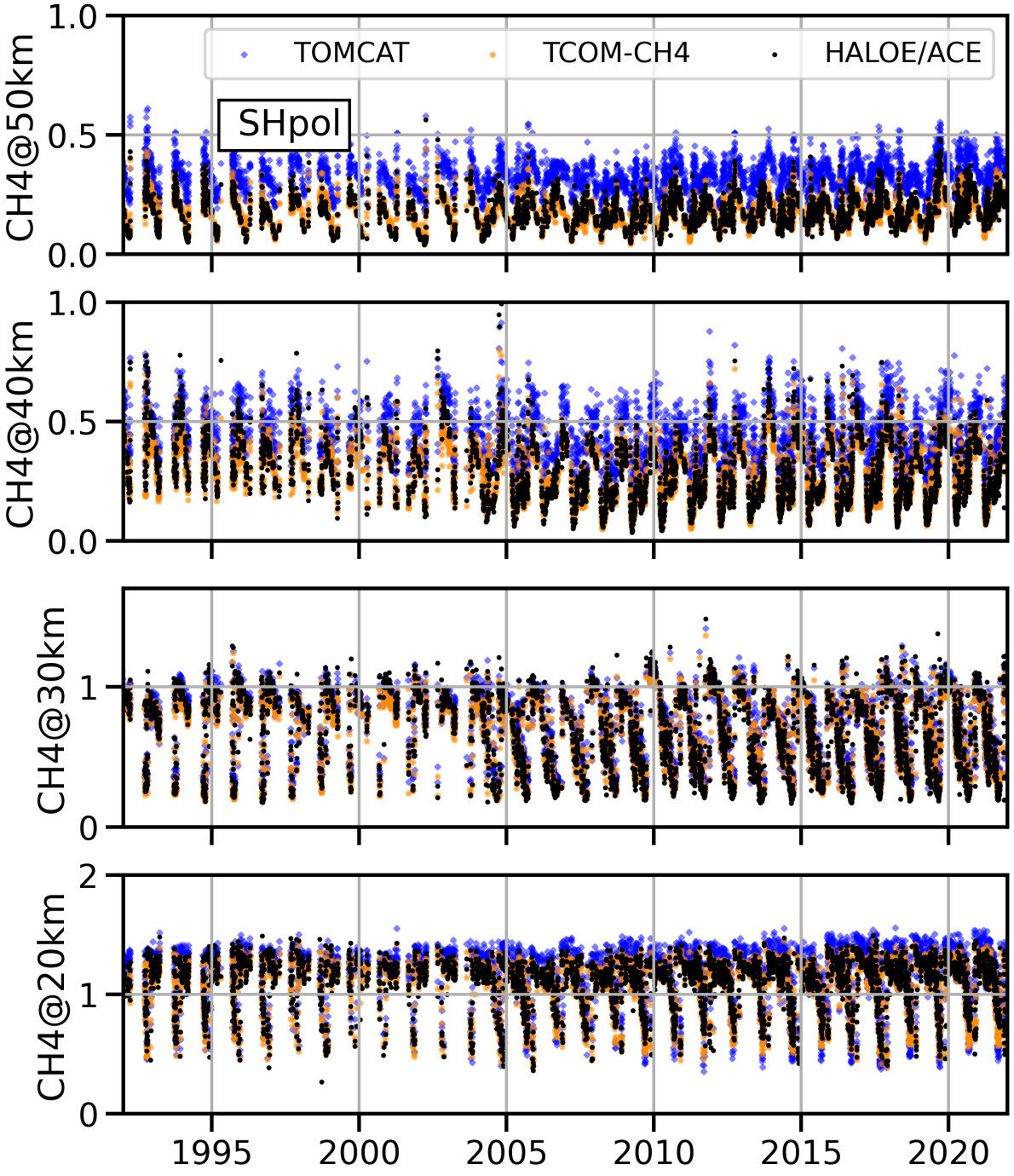

Figure 4. Time evolution (1992-2021) of CH_4 (in ppm) from TOMCAT (blue crosses), TCOM-CH4 (orange diamonds) and satellite data (black dots) for SHpol (50°S–90°S) at 20, 30, 40 and 50 km. Note that for clarity only 10% (every 10th) of data points are shown. Due to sharp gradient in vertical distribution, the y axis range varies between the panels.

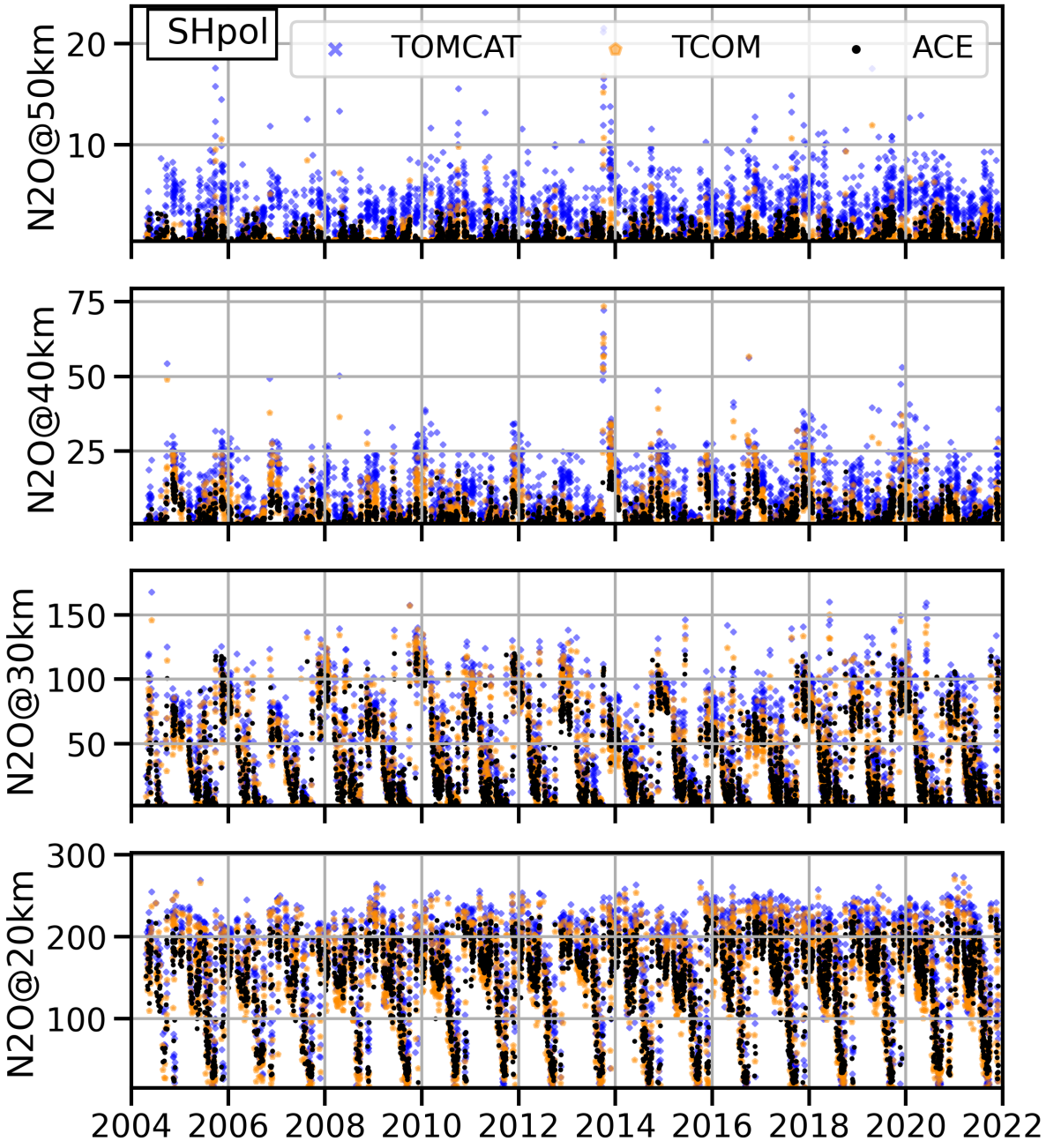

Figure 5. Same as Figure 4, but for N_2O (in ppb). The comparison is shown for the 2004-2021 time period.

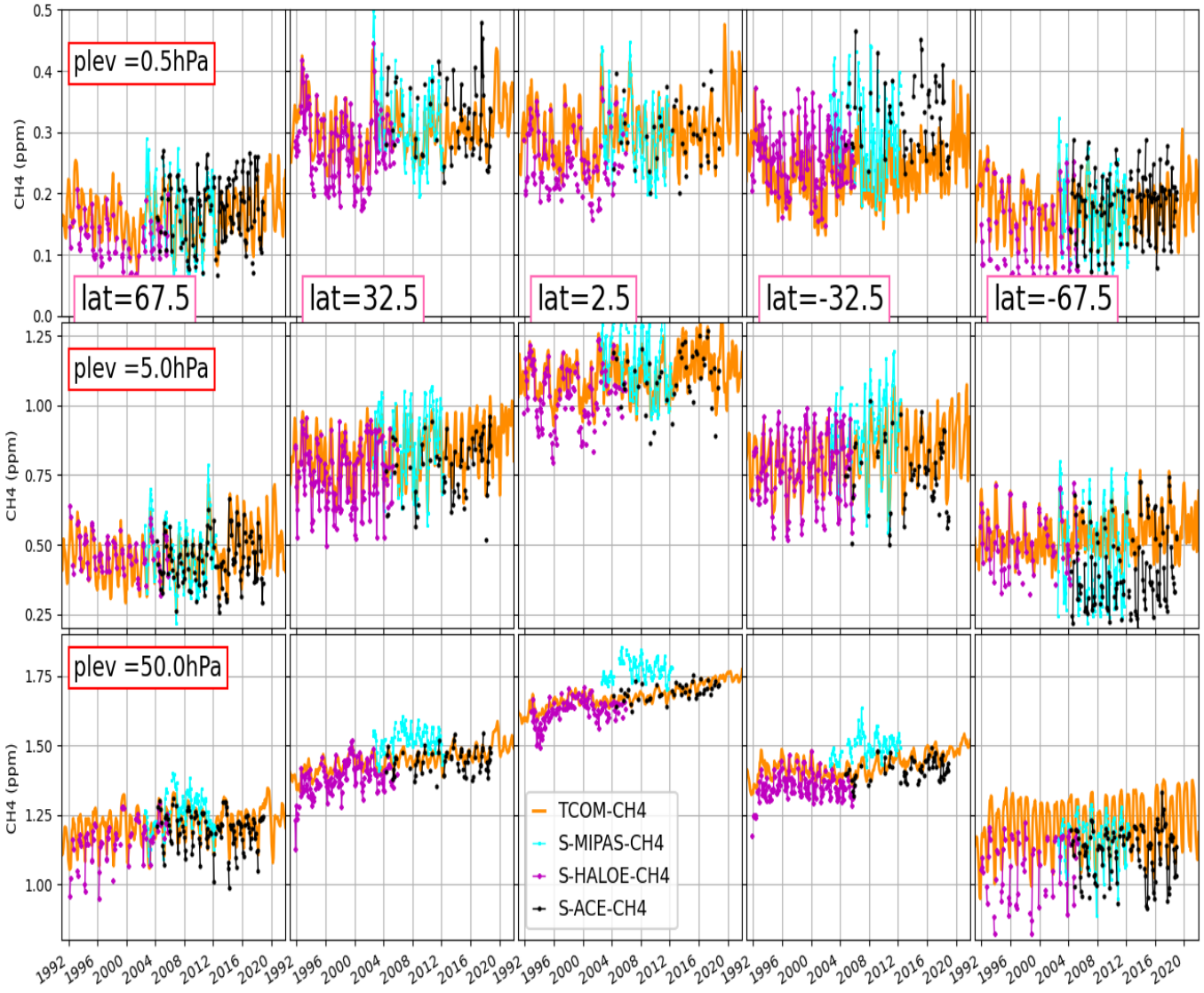

Figure 6. Comparison between TCOM-CH4 (dark line) and three (ACE (black line), HALOE (magenta line) and MIPAS (aqua line)) satellite instrument-based SPARC-CH4 data set (for details see Hegglin et al. (2021)). Time series of monthly mean values from SPARC-CH4 and TCOM-CH4 data set are shown for 0.5 hPa (top), 5 hPa (middle), and 50 hPa (bottom) for five latitude bins: 67.5° and 32.5° in both the hemispheres as well as 2.5°N (middle).

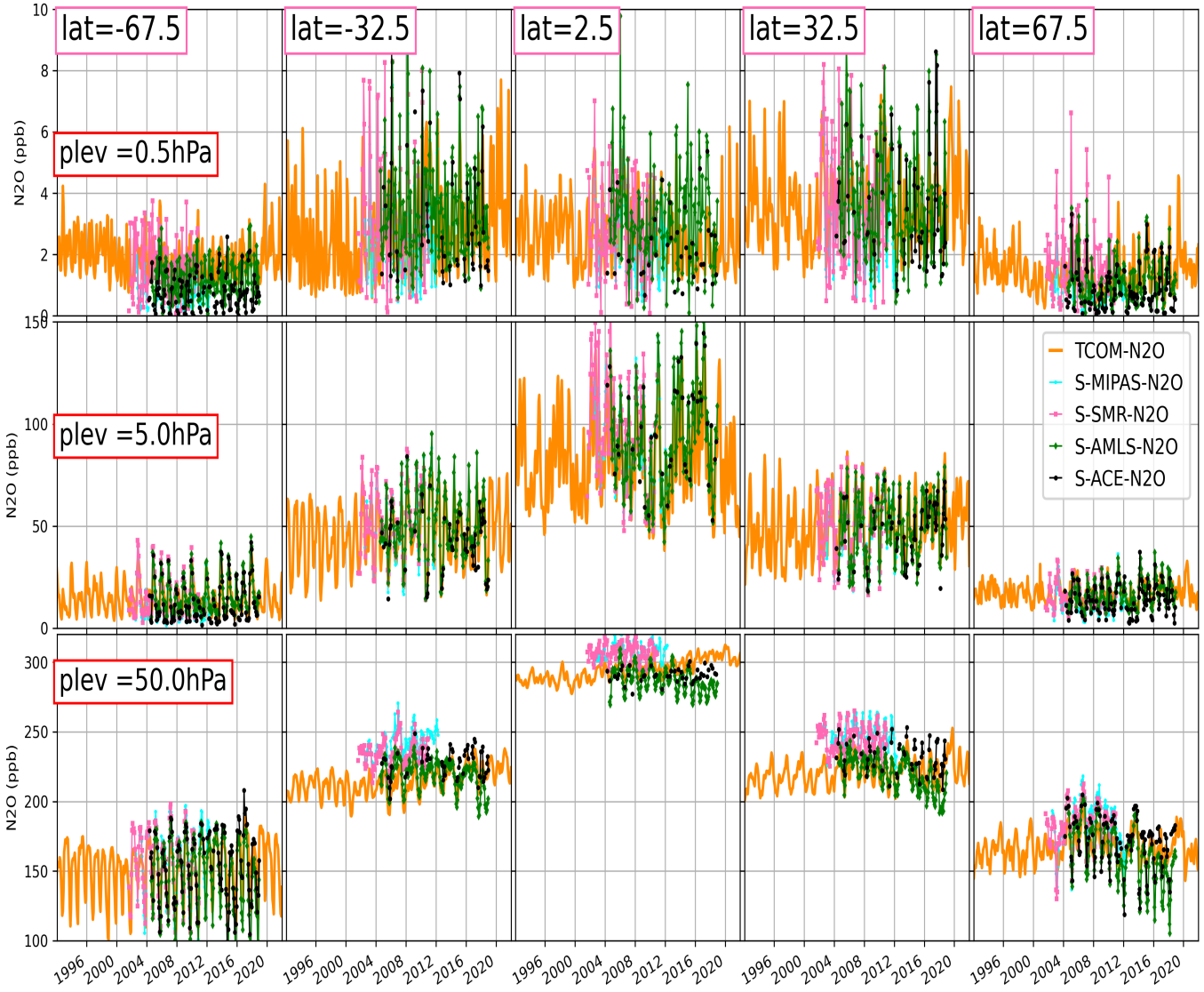

Figure 7. Same as Figure 6 but for N_2O. SPARC data from the four satellite instruments ACE (v3.6), Aura-MLS (v4), MIPAS (v422) and SMR (v2.1) are shown with black, green, aqua and pink coloured lines, respectively.

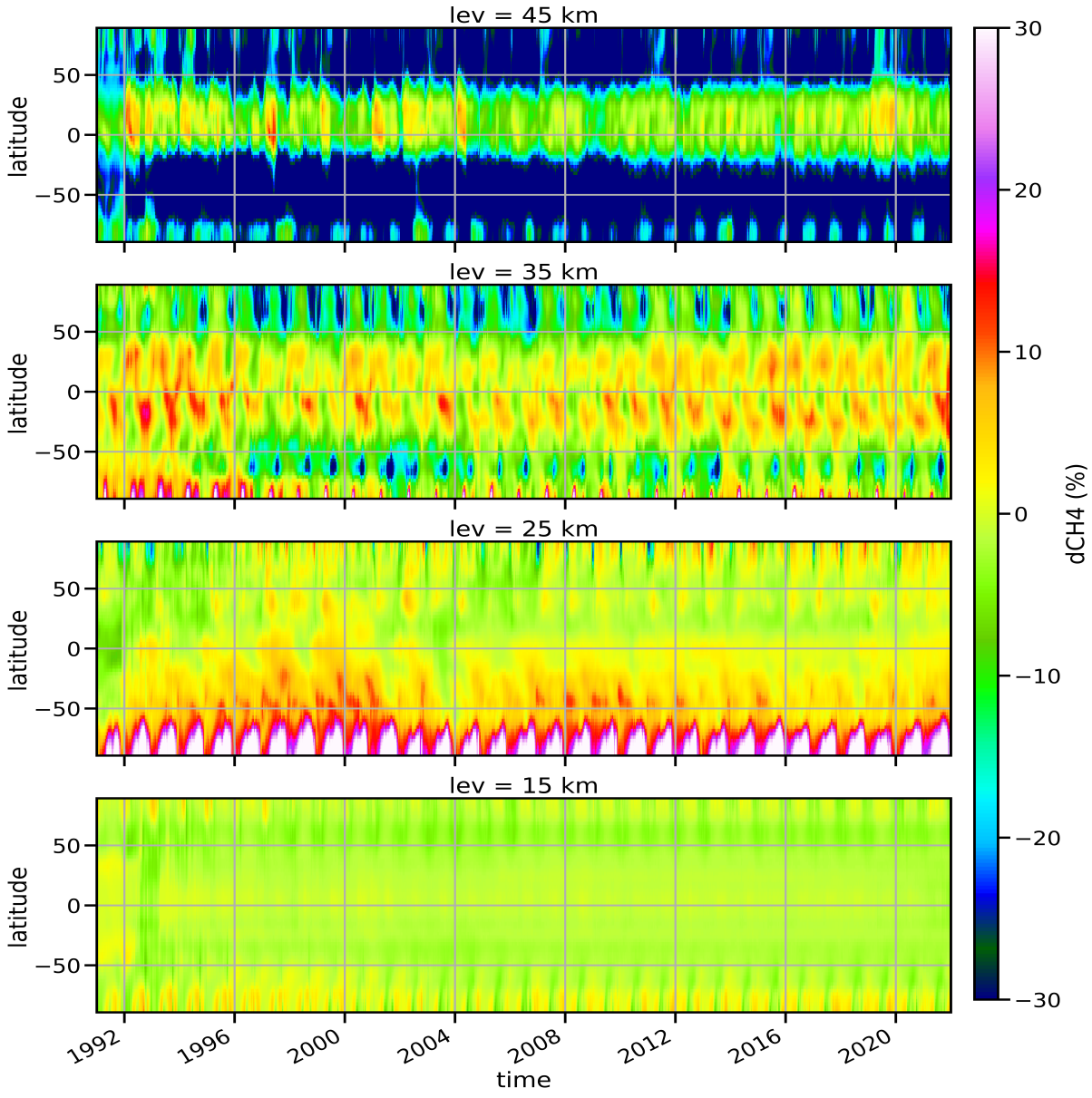

Figure 8. Latitude-time cross section of the differences between TCOM-CH4 and TOMCAT CTM CH_4 profiles (in %) at 15 km (bottom), 25 km, 35 km and 45 km (top). Percent differences are calculated as 200 × (TCOM-TOMCAT)/(TCOM-TOMCAT).